ACS APPLIED MATERIALS & INTERFACES

Research Article

www.acsami.org

Hollow Sn–SnO_2 Nanocrystal/Graphite Composites and Their Lithium Storage Properties

Youngmin Lee,[†,‡] Mi Ru Jo,[†] Kyeongse Song,[†] Ki Min Nam,[§] Joon T. Park,[§] and Yong-Mook Kang*[,†]

[†]Department of Chemistry, Dongguk University-Seoul, Seoul, 100-715, Republic of Korea

[‡]Division of Materials Science and Engineering, Hanyang University, Seoul, 133-791, Republic of Korea

[§]Department of Chemistry, Korea Advanced Institute of Science and Technology (KAIST), Daejeon, 305-701, Republic of Korea

Supporting Information

ABSTRACT: Hollow spheres have been constructed by applying the Kirkendall effect to Sn nanocrystals. This not only accommodates the detrimental volume expansion but also reduces the Li^+ transport distance enabling homogeneous Li–Sn alloying. Hollow Sn–SnO_2 nanocrystals show a significantly enhanced cyclic performance compared to Sn nanocrystal alone due to its typical structure with hollow core. Sn–SnO_2/graphite nanocomposites obtained by the chemical reduction and oxidation of Sn nanocrystals onto graphite displayed very stable cyclic performance thanks to the role of graphite as an aggregation preventer as well as an electronic conductor.

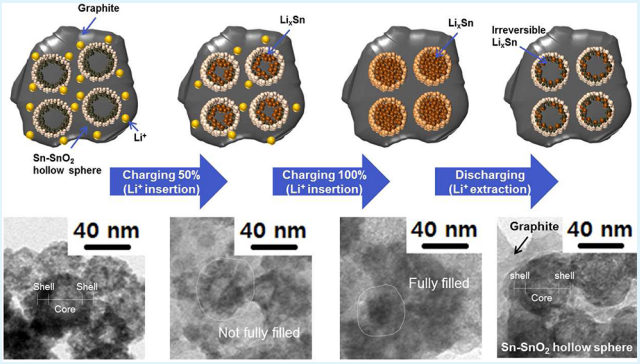

KEYWORDS: *Kirkendall effect, hollow core, volume expansion, SnO_2, anode, lithium rechargeable battery*

INTRODUCTION

Metal oxides are an important group of materials because they form a wide variety of structures, display many interesting properties, and have numerous applications.[1−4] In particular, various metal oxides including transition metal oxides, tin oxides, and silicon oxides have attracted great interest in their potential applications as catalysts, magnetic data storage devices, lithium-ion battery materials, and solid-state sensors.[5−9] Among them, SnO_2 has been more intensively investigated due to its typical semiconducting character with a wide band gap (E_g = 3.6 eV). As an alternative anode material for lithium-ion batteries, SnO_2-based materials have displayed very promising properties such as high capacity, which may enable them to substitute for the commercialized anode material, graphite, in spite of the initial irreversible capacity induced by Li_2O formation and the abrupt capacity fading caused by volume expansion during cycling. To minimize such a drastic volume change, the particle size and morphology of SnO_2 have been controlled by adopting various synthetic methods including chemical vapor deposition (CVD), templated sol–gel process,[10] surfactant-controlled polyol process, and so on. Nanotubes, nanowires, and nanorods obtained from these processes showed significant electrochemical improvement compared to nanocrystals, but its anodic performance other than the specific capacity was still far behind that of the commercial anode material, graphite.[11−16] However, because the mechanical failure and electrochemical decay of SnO_2 nanomaterials for lithium ion batteries originate from not only volume expansion itself but also particle agglomeration worsening their pulverization during Li^+ insertion/extraction, particle size and pore concentration need to be properly controlled in the SnO_2 nanostructure supported by a free-standing matrix.

Surfactant-assisted processes generally provide outstanding control over the particle size of metal oxide or metal nanocrystals, leading to almost perfectly monodispersed samples. Composites based on metal or alloys and graphite have been extensively studied since graphite can play a role of adsorbing material to prevent agglomeration or size growth of nanocrystals as well as supply kinetically unlimited electron transport.[17−22] A hollow core inside nanocrystals can offer enough space for accommodating the detrimental volume expansion and kinetic enhancement attributed to the shortened distance for Li^+ transport. Hence, the limited size growth by utilizing proper surfactants, the role of graphite as an adsorber or electronic conductor, and the fabrication of an internal hollow structure are essential to counteracting the mechanical failure and electrochemical decay of SnO_2 nanomaterials.[23−29]

Herein, we report a synergetic strategy based on a surfactant-assisted process for nanoscale control of Sn, the versatility of graphite for adsorption of nanocrystals and their facilitated electron transport, and the Kirkendall effect governing the oxidation process of Sn nanocrystals for a well constructed hollow structure. Consequently, we demonstrate that Sn–SnO_2

Received: March 24, 2012
Accepted: June 18, 2012
Published: June 18, 2012

nanocrystal/graphite with a hollow core can be successfully synthesized and displays high lithium storage capacity with fair reversibility up to the 50th cycle.

EXPERIMENTAL SECTION

Preparation of Sn Nanocrystals. Sn nanocrystals were synthesized by a chemical reduction method as follows: Sn precursor solution was prepared by dissolving 0.2 g of $SnCl_2{\cdot}2H_2O$ (Aldrich) and 0.01 g of Poly(vinylpyrrolidone) (M_w = 55 000, Aldrich) as surfactant in a mixture of distilled water (25 mL). The solution was rapidly reacted by 0.067 g of $NaBH_4$ (Aldrich) as reducing agent with vigorous stirring during 10 min. To remove impurities, the final product was washed with ethyl alcohol via centrifugal process and dried at 60 °C for 6 h in a vacuum oven.

Preparation of Sn/Graphite Nanocomposites. Sn/graphite nanocomposites were prepared via dropwise method as follows: Sn solution was prepared by dispersing synthesized Sn in ethyl alcohol (15 mL). Then, graphite solution was prepared by dispersing 0.2 g of graphite powder (~ 100 μm, Kanto chemical) in ethyl alcohol (15 mL) with vigorous stirring for 30 min. The Sn solution was added to the graphite solution dropwise and kept under continuous vigorous stirring for 24 h. The product was washed with ethyl alcohol via centrifugal process and dried at 60 °C for 6 h in a vacuum oven.

Preparation of Sn−SnO_2 or Sn−SnO_2/Graphite Composites. Sn was oxidized using Kirkendall effect. The solution was prepared by dispersing unwashed Sn nanocrystals or Sn/graphite nanocomposites in distilled water (30 mL). The solution was stirred under an O_2 (99.9%) atmosphere at room temperature during different times. Then the product was washed with ethyl alcohol via centrifugal process and dried at 60 °C for 6 h in a vacuum oven.

Electrochemical Experiments. To make an electrode for electrochemical measurements, a mixture of 75 wt % of the active material and 17 wt % acetylene black was added to a solution containing 8 wt % polyvinylidene fluoride (PVDF) in *n*-methyl-2-pyrolidinone (NMP). This slurry was pasted onto a copper foil current collector and dried at 120 °C for 5 h in vacuum (10^{-3} Torr). After pressing under a pressure at about 5000 psi, half cells (CR 2016 coin-type) were fabricated to evaluate the anodic performance of the Sn based nanocomposites. The assembly was carried out in an Ar-filled glovebox with less than 10 ppm each of oxygen and moisture. A Li metal foil was used as the counter and reference electrode, and 1 M $LiPF_6$ dissolved in a 1:1 (v/v) mixture of ethylene carbonate (EC) and diethylene carbonate (DEC) was employed as the electrolyte. Charge−discharge tests were performed up to the fiftieth cycle in the range of 0.05 to 1.5 V (vs Li/Li^+). The current density was 57.8 mAh/g, which corresponds to about 0.1 C when considering the composition of Sn−SnO_2 nanocrystal/graphite composites.

Structural and Morphological Characterization. The microstructure and morphology of Sn-based nanocomposites were characterized by X-ray diffraction (Rigaku D/Max-RB diffractometer, using Cu Kα radiation at 40 kV and 100 mA) and high-resolution transmission electron microscopy (Philips F20Tecai operated at 200 kV)

RESULTS AND DISCUSSION

Figure 1 shows the X-ray diffractogram of Sn nanocrystals, Sn−SnO_2 nanocrystals obtained through the oxidation of Sn nanocrystals, and their composites with graphite. When $SnCl_2{\cdot}2H_2O$ was reduced by $NaBH_4$, the diffraction pattern well matched with the single-crystalline metallic Sn which belongs to the space group I41/amd. The average size of Sn nanocrystals, calculated by fitting the relatively large diffraction peaks assigned to (2 0 0), (1 0 1) (2 1 1), and (2 2 0) planes using Scherrer's equation, was 30−40 nm, which was in an approximate agreement with that observed by TEM analysis. When the oxidation time for Sn nanocrystals was increased from 3 to 11 h, the peaks indexed to metallic Sn faded out with

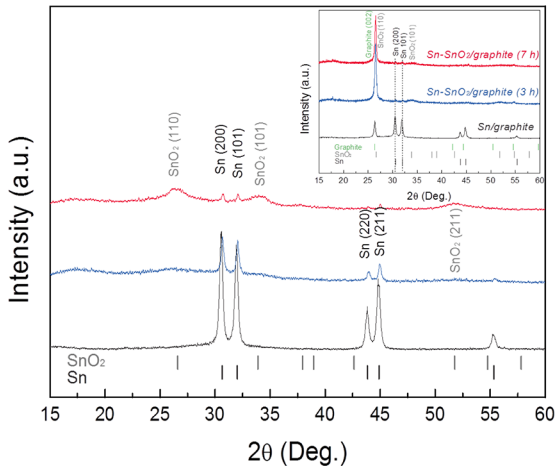

Figure 1. XRD patterns of Sn nanocrystals (black line) and Sn−SnO_2 nanocrystals obtained by oxidation for 3 h (blue line) and 7 h (red line). Inset figure corresponds to XRD patterns of Sn nanocrystals/graphite composites and Sn−SnO_2 nanocrystals/graphite composites with different oxidation times.

the evolution of SnO_2. According to Scherrer's equation, the average size of SnO_2 is approximately 1.2 or 2.0 nm depending on the oxidation time. Based on this, we could expect that metallic Sn gradually changes to SnO_2. In the inset of Figure 1, XRD patterns of Sn nanocrystal/graphite composites and the oxidized Sn nanocrystal/graphite composites are comparatively shown. Even if graphite generally encourages a reductive atmosphere, the oxidation tendency of Sn/graphite hardly differs from that of Sn. Consequently, the ratio of SnO_2 to Sn is almost proportionally changed as the oxidation time increases as clearly shown in Figure S1 in the Supporting Information. When Sn nanocrystals and Sn nanocrystal/graphite composites were oxidized for 9 h, XRD patterns attributed to metallic Sn commonly disappeared with the evolution of SnO_2.

Figure 2 directly shows how metallic Sn in Sn nanocrystals or Sn nanocyrstal/graphite composites change into SnO_2. Figure 2a−c provide a clear view on the oxidation process of Sn nanocrystals including hollow core. Before oxidation, Sn nanocrystals have a round shape with immaculate surface, but much smaller particles appearing as agglomerates form at the

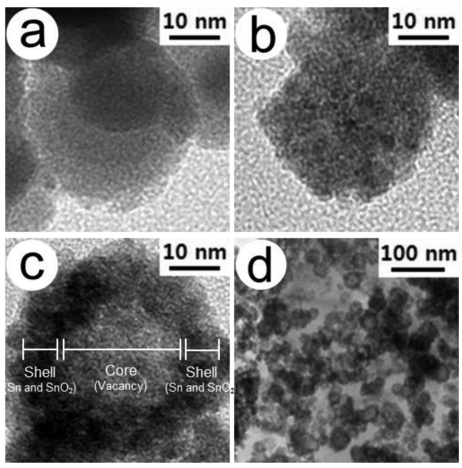

Figure 2. TEM images of Sn−SnO_2 nanocrystals with hollow core oxidized for (a) 0 h, (b) 3 h, (c) 7 h, and TEM image of (d) Sn−SnO_2 nanocrystals/graphite composites oxidized for 7 h.

dx.doi.org/10.1021/am3005237 | ACS Appl. Mater. Interfaces 2012, 4, 3459−3464

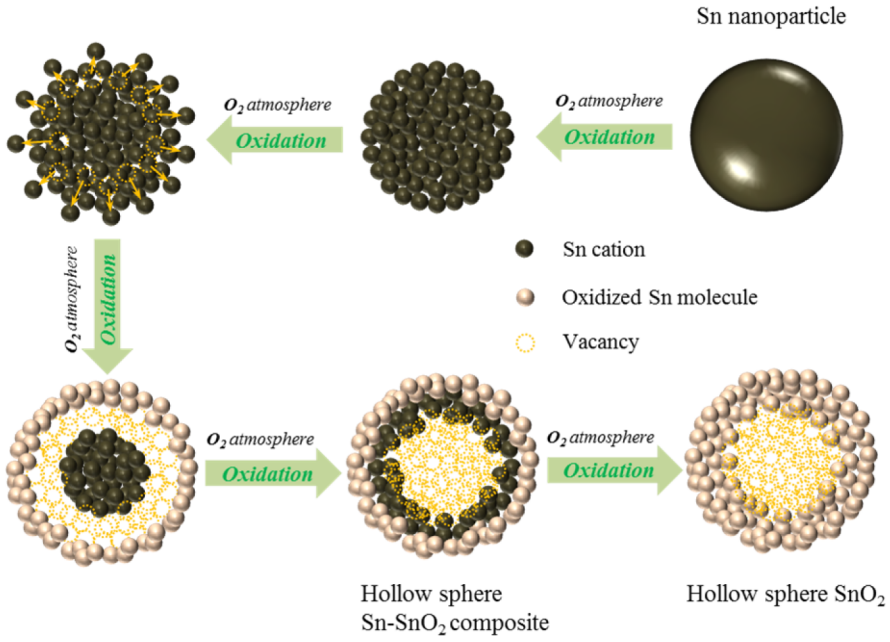

Figure 3. Schematic illustration of hollow core evolution in the oxidized Sn nanocrystals dominated by Kirkendall effect.

beginning of oxidation (Figure 2b). After the oxidation for 7 h, vacancies converge into a huge hollow core inside nanocrystals. Herein, the introduction of the hollow core is accompanied by the phase change from metallic Sn to SnO_2 in the shell as indicated by XRD results in Figure 1. Because the size (below 2 nm) of the smaller particles evolved after 7 h oxidation is almost in accordance with the particle size of SnO_2 calculated from its XRD patterns, the main component of shell can be attributed to SnO_2. When Sn nanocrystals are exposed under O_2 ambient, their oxidation seems to be dominated by Kirkendall effect, which is the first experimental proof indicating that atomic diffusion occurs not through the direct exchange of atoms but by vacancy exchange. The net direction of the flow of atoms is balanced by an opposite flow of vacancies, which tend to condense into voids or annihilate at dislocations.

Figure 3 explains how voids are made by Kirkendall effect resultantly evolving $Sn-SnO_2$ nanocomposites with hollow core. When Sn nanocrystals undergo oxidation, the high surface-to-volume ratio of nanocrystals markedly increases the net rate of vacancy injection. Within the small volume of a transforming nanocrystal, the supersaturated vacancy cloud tends to coalesce into a single void. Because the uniformity of voids is closely related to that of the starting materials, we could produce a relatively uniform population of hollow $Sn-SnO_2$ nanostructures with monodisperse Sn nanocrystals. Figure 2d shows that Sn nanocrystal/graphite composites undergo an oxidation process similar to Sn nanocrystals. The more detailed observation with the oxidation time confirms that Kirkendall effect is the main formation mechanism for $Sn-SnO_2$ nanocrystals or $Sn-SnO_2$ nanocrystal/graphite composites with a hollow core (Figures S2 and S3).

To obtain more information on the chemical states of the $Sn-SnO_2$ nanocrystals and $Sn-SnO_2$ nanocrystal/graphite composites, XPS analysis was conducted. Figure 4 includes O 1s spectra and Sn 3d spectra for $Sn-SnO_2$ and the $Sn-SnO_2$/graphite composite. After the oxidation of Sn nanocrystals, the O 1s binding energy of $Sn-SnO_2$ is 532.1 eV, which

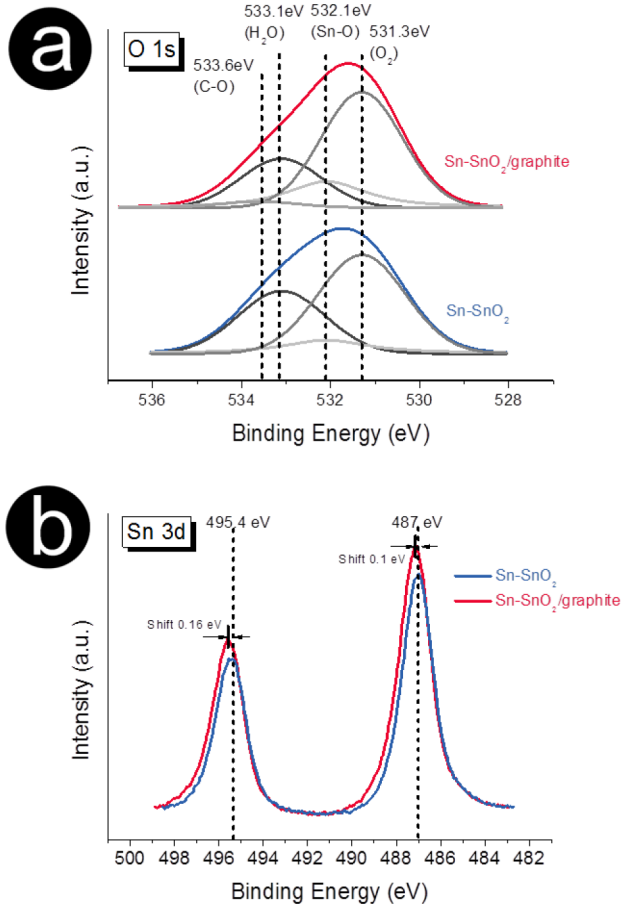

Figure 4. (a) XPS O 1s narrow scan spectra for $Sn-SnO_2$ nanocrystals and $Sn-SnO_2$ nanocrystal/graphite composites, and (b) XPS Sn 3d narrow scan spectra for $Sn-SnO_2$ nanocrystals and $Sn-SnO_2$ nanocrystal/graphite composites.

corresponds to the binding energy of Sn−O bonding. On the other hand, the O 1s spectrum of the composites is convoluted

dx.doi.org/10.1021/am3005237 | ACS Appl. Mater. Interfaces 2012, 4, 3459−3464

from not only Sn−O bonding but also a positively shifted aliphatic C−O bonding, which is located around 533.6 eV. O_2 and H_2O bondings are attributed to the adsorbed H_2O and O_2 on graphite. The bonding nature between C and SnO_2 was determined from Sn 3d spectrum as well as C1s spectra. If the Sn in the Sn−SnO_2 nanocrystal/graphite composites were directly bonded to C atoms, novel peaks attributed to Sn−C bonding should be located on the left-hand side of the Sn $3d_{3/2}$ peak and the Sn $3d_{5/2}$ peak, respectively. However, the Sn 3d spectra of the Sn−SnO_2 nanocrystal/graphite composites show only a little positive peak shifting associated with the inductive effect of C−O bonding reducing the electron density in the d orbitals of Sn. Hence, we can surmise that Sn−SnO_2 nanocrystal tends to be bonded to graphite through not Sn−C bonding but through C−O bonding. C 1s spectra also shows that most of the carbon tends to be bonded to the oxygen dangling bond of SnO_2 (Figure S4).

Figure 5 compares the electrochemical performances of Sn nanocrystals, Sn nanocrystal/graphite composites, Sn−SnO_2 nanocrystals, and Sn−SnO_2 nanocrystal/graphite composites. Their initial galvanostatic profiles are shown in Figure 5a, in which the voltage was varied from 0.05 to 1.5 V vs Li/Li^+. The galvanostatic profile of Sn nanocrystals shows clear multistep voltage plateaus during Li^+ insertion/extraction which are indicative of traces of phase transitions between the Li−Sn intermetallic compounds, whereas its composite with graphite, Sn−SnO_2 nanocrystals, and Sn−SnO_2 nanocrystals/graphite composites display sloping voltage profiles. The reason graphite was used for the composites with Sn nanocrystals and Sn−SnO_2 nanocrystals is the high surface free energy of the nanocrystals, leading to aggregation during electrochemical alloying or dealloying with Li^+ and consequently worsening their electrochemical properties. Figure 5b shows the cyclic performances of Sn nanocrystals, Sn−SnO_2 nanocrystals, and their composites with graphite. Even if the first discharge capacity of Sn nanocrystals came to 596 mAh/g, further cycling led to a drastic capacity decay to 49 mAh/g after 50 cycles. Meanwhile, Sn−SnO_2 nanocrystals exhibit a clear cyclic enhancement compared to Sn nanocrystals, but the drastic capacity decay within a few cycles is also inevitable. Because graphite can play the role of free-standing matrix constraining the aggregation of nanocrystals, the electrochemical properties of Sn−SnO_2 nanocrystals could be properly compared with those of Sn nanocrystals by fabricating the composites between nanocrystals and graphite. Figure 5b and its inset figure indicate the electrochemical superiority of Sn−SnO_2 nanocrystal/graphite composites by comparing its cyclic retention and Coulombic efficiency with those of Sn nanocrystal/graphite composites. Herein, because the electrochemical superiority of Sn−SnO_2 nanocrystal/graphite composites to Sn nanocrystal/graphite composites is mainly attributed to the physical difference between Sn nanocrystal and Sn−SnO_2 nanocrystal, the morphological and crystallographic changes of Sn−SnO_2 nanocrystals were observed during charge/discharge.

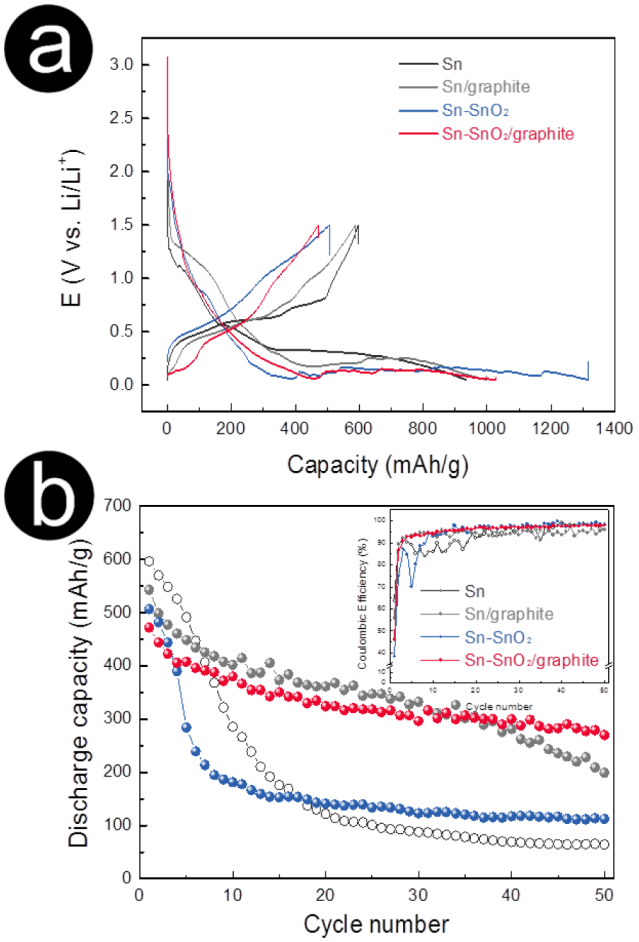

Figure 5. Anodic performances of as-synthesized Sn and Sn-based composite; (a) the initial galvanostatic charge/discharge profiles between 0.05 and 1.5 V, and (b) the cyclic performance of as-synthesized Sn and Sn-based composites up to the fiftieth cycle.

TEM images in Figure 6 illustrate the morphological changes of Sn−SnO_2 nanocrystal/graphite composites during charge/discharge at the initial cycle. Before the electrochemical reaction, Sn−SnO_2 nanocrystals include a hollow core at its center (Figure 6a), but its characteristic hollow structure gradually disappears due to the inward volume expansion of Sn−SnO_2 shell as Li^+ insertion into Sn−SnO_2 nanocrystals proceeds. After the full reaction with Li^+ (Figure 6c), only solid

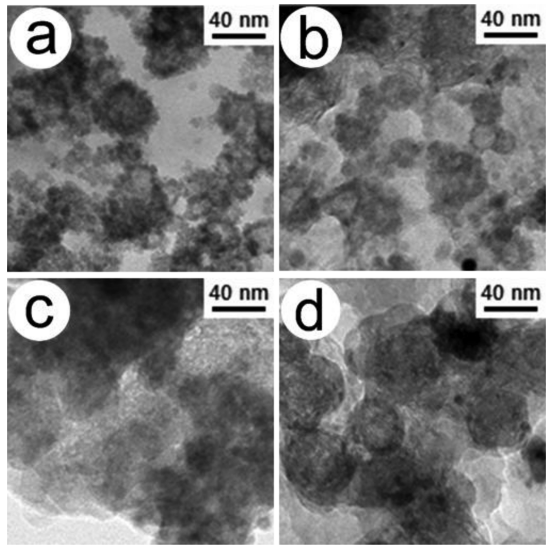

Figure 6. TEM images of Sn−SnO_2 nanocrystal/graphite composites after charge or discharge: (a) as synthesized, (b) after 50% charge (Li^+ insertion), (c) after 100% charge, and (d) after 100% discharge (Li^+ extraction).

dx.doi.org/10.1021/am3005237 | ACS Appl. Mater. Interfaces 2012, 4, 3459−3464

spheres are observed, proving that the void inside the Sn−SnO_2 nanocrystal accommodates the detrimental volume expansion of Sn or SnO_2 when alloying with Li^+. Interestingly, the hollow core emerges again without any other apparent physical change after the depletion of Li^+ indicating the superb reversibility of charge−discharge reaction between Li^+ and Sn−SnO_2 nanocrystal having the hollow structure (Figure 6d). Figure S7 demonstrates the positive effect of the hollow structure on the morphological changes of Sn−SnO_2 nanocrystal/graphite composites. Herein, the morphological comparison between the charged electrode and the discharged electrode at first cycle clearly shows that Sn−SnO_2 nanocrystal/graphite composites undergo less physical change associated with volume expansion than Sn nanocrystal/graphite composites. Finally, XRD analyses (Figure S8) were conducted to figure out the crystallographic change associated with morphological changes. Because the cycled electrodes were sealed with Sellotape to prevent air exposure, the peak related to Sellotape is commonly observed around 26°. The drastically reduced Sn peak intensity between first cycle and 10th cycle in Sn nanocrystal/graphite composites proves that the composite has to undergo a pulverization induced by the volume expansion during Li^+ insertion. Meanwhile, Sn−SnO_2 nanocrystal/graphite composites do not have any distinct change in the peaks related to Sn or SnO_2. If graphite in each composite participates in charge/discharge process, the interplanar spacing ($d_{(002)}$) of its prismatic plane should be changed. Because the (002) peak of graphite keeps up its initial position even during charge/discharge, the primary role of graphite in Sn/graphite composites and Sn−SnO_2/graphite is not participating in the electrochemical reaction, but enabling Sn nanocrystals or Sn−SnO_2 nanocrystals to retain their electrochemical reactivity. These consecutive analytic results based on TEM, SEM, and XRD obtained from cycled electrodes or materials clearly stress the significance of a hollow structure as the accommodator of volume expansion for the electrochemical superiority of Sn−SnO_2 nanocrystal/graphite composites.

CONCLUSION

The general methods for fabricating hollow metal oxide spheres have included templates to guide its characteristic hollow structure. On the other hand, we synthesized Sn−SnO_2 nanocrystals with hollow core via the oxidation process dominated by Kirkendall effect without any kind of template. Herein, a novel inside-out Ostwald ripening mechanism is proposed to account for the template-free formation of Sn−SnO_2 hollow spheres. By comparing the electrochemical properties and morphological changes of hollow Sn−SnO_2 nanocrystals with those of Sn nanocrystals on graphite acting as an aggregation preventer, it could be shown that the void provided by Kirkendall effect efficiently accommodates the detrimental volume expansion of Sn or SnO_2 for the electrochemical superiority of hollow Sn−SnO_2 nanocrystal/graphite composites.

ASSOCIATED CONTENT

Supporting Information

This material is available free of charge via the Internet at http://pubs.acs.org.

AUTHOR INFORMATION

Corresponding Author

*E-mail: dake1234@dongguk.edu.

Notes

The authors declare no competing financial interest.

ACKNOWLEDGMENTS

This work was supported by the National Research Foundation of Korea funded by the Ministry of Education, Science, and Technology (NRF-2010-C1AAA001-0029018), and the Fundamental R&D Program for Technology of World Premier Materials funded by the Ministry of Knowledge Economy (grant 10037918).

REFERENCES

(1) Wang, Z. L.; Song, J. *Science* **2006**, *312*, 242−246.
(2) Subramanian, V.; Wolf, E. E.; Kamat, P. V. *J. Am. Chem. Soc.* **2004**, *126*, 4943−4950.
(3) Seo, W. S.; Jo, H. H.; Lee, K.; Kim, B.; Oh, S. J.; Park, J. T. *Angew. Chem., Int. Ed.* **2004**, *43*, 1115−1117.
(4) Lou, X. W.; Chen, J. S.; Chen, P.; Archer, L. A. *Chem. Mater.* **2009**, *21*, 2868−2874.
(5) Li, W.-Y.; Xu, L.-N.; Chen, J. *Adv. Funct. Mater.* **2005**, *15*, 851−857.
(6) Wang, G.; Shen, X.; Horvat, J.; Wang, B.; Liu, H.; Wexler, D.; Yao, J. *J. Phys. Chem. C* **2009**, *113*, 4357−4361.
(7) Binotto, G.; Larcher, D.; Prakash, A. S.; Urbina, R. H.; Hegde, M. S.; Tarascon, J.-M. *Chem. Mater.* **2007**, *19*, 3032−3040.
(8) Choi, H. C.; Lee, S. Y.; Kim, S. B.; Kim, M. G.; Lee, M. K.; Shin, H. J.; Lee, J. S. *J. Phys. Chem. B* **2002**, *103*, 9252−9260.
(9) Nam, H.-J.; Sasaki, T.; Koshizaki, N. *J. Phys. Chem. B* **2006**, *110*, 23081−23084.
(10) Li, N.; Martin, C. R. *J. Electrochem. Soc.* **2001**, *148*, A164−A170.
(11) Park, J. W.; Rajendran, S.; Kwon, H. S. *J. Power Sources* **2006**, *159*, 1409−1415.
(12) Idota, Y.; Kubota, T.; Matsufuji, A.; Maekawa, Y.; Miyasaka, T. *Science* **1997**, *276*, 1395−1397.
(13) Poizot, P.; Laruelle, S.; Grugeon, S.; Dupont, L.; Tarascon, J.-M. *Nature* **2000**, *407*, 496−499.
(14) Park, M. S.; Kang, Y. M.; Wang, G. X.; Dou, S. X.; Liu, H. K. *Adv. Funct. Mater.* **2008**, *18*, 455−461.
(15) Noh, M. J.; Kwon, Y. J.; Lee, H. J.; Cho, J. P.; Kim, Y. J.; Kim, M. G. *Chem. Mater.* **2005**, *17*, 1926−1929.
(16) Park, M. S.; Wang, G. X.; Kang, Y. M.; Wexler, D.; Dou, S. X.; Liu, H. K. *Angew. Chem., Int. Ed.* **2007**, *46*, 750−753.
(17) Fan, J.; Wang, T.; Yu, C.; Tu, B.; Jiang, Z.; Zhao, D. *Adv. Mater.* **2004**, *16*, 1432−1436.
(18) Liu, J.; Li, W.; Manthiram, A. *Chem. Commun.* **2010**, *46*, 1437−1439.
(19) Chang, C. C.; Liu, S. J.; Wu, J. J.; Yang, C. H. *J. Phys. Chem. C* **2007**, *111*, 16423−16427.
(20) Wang, Y.; Lee, J. Y. *Electrochem. Commun.* **2003**, *5*, 292−296.
(21) Park, M. S.; Kang, Y. M.; Dou, S. X.; Liu, H. K. *J. Phys. Chem. C* **2008**, *112*, 11286−11289.
(22) Yin, Y. D.; Rioux, R. M.; Erdonmez, C. K.; Hughes, S.; Somorjai, G. A.; Alivisatos, A. P. *Science* **2004**, *304*, 711−714.
(23) Zhao, Q.; Xie, Y.; Dong, T.; Zhang, Z. *J. Phys. Chem. C* **2007**, *111*, 11598−11603.
(24) Lee, K. T.; Lee, Y. S.; Oh, S. M. *J. Am. Chem. Soc.* **2003**, *125*, 5652−5653.
(25) Deng, D.; Lee, J. Y. *Chem. Mater.* **2008**, *20*, 1841−1846.
(26) Han, S. J.; Jang, B. C.; Kim, T. A.; Oh, S. M.; Hyeon, T. H. *Adv. Funct. Mater.* **2005**, *15*, 1845−1850.
(27) Lou, X. W.; Wang, Y.; Yuan, C.; Lee, J. Y.; Archer, L. A. *Adv. Mater.* **2006**, *18*, 2325−2329.
(28) Sun, X.; Liu, J.; Li, Y. *Chem.—Eur. J.* **2006**, *12*, 2039−2047.

(29) Besenhard, J. O.; Yang, J.; Winter, M. *J. Power Sources* **1997**, *68*, 87−90.